





# A novel photoluminescence hyperspectral camera for the study of artworks

Marta Ghirardello<sup>1</sup> , Cristian Manzoni<sup>2</sup>, Michele Gironda<sup>3</sup>, Roberto Alberti<sup>3</sup>, Roland Lenz<sup>4</sup>, Judit Zöldföldi<sup>5</sup>, Sonja Behrendt<sup>6</sup>, Boaz Paz<sup>6</sup>, Gianluca Valentini<sup>1,2</sup>, Daniela Comelli<sup>1,a</sup> 

<sup>1</sup> Physics Department, Politecnico Di Milano, Piazza Leonardo da Vinci 32, 20133 Milan, Italy

<sup>2</sup> IFN, CNR, Piazza Leonardo da Vinci 32, 20133 Milan, Italy

<sup>3</sup> XGLab S.R.L.- Bruker Nano Analytics, Via Conte Rosso 23, 20134 Milan, Italy

<sup>4</sup> Institute for Conservation Sciences, Staatliche Akademie der Bildenden Künste, Am Weißenhof 1, 70191 Stuttgart, Germany

<sup>5</sup> University of Stuttgart, Materials Testing Institute, Pfaffenwaldring 2b, 70569 Stuttgart, Germany

<sup>6</sup> Paz Laboratorien Für Archäometrie, Planiger Straße 34/Haus 18/19, 55543 Bad Kreuznach, Germany

Received: 19 May 2021 / Accepted: 3 October 2021

© The Author(s) 2021

**Abstract** We present the application of a novel hyperspectral camera, based on the Fourier-transform approach, to study the photoluminescence emission from artworks at different spatial scales and emission timescales. The hyperspectral system relies on an innovative wide-field, compact and ultra-stable interferometer coupled to different excitation and detection methods. Here, we describe and illustrate the potentialities and limitations of its use when coupled with excitation at variable fluence and with time-gated detection. The developed methods allow an in-depth characterization of the optical emission from luminescent materials in cultural heritage and provide information on the nature of the recombination pathways in crystalline pigments. Indeed, one of the main difficulties in the interpretation of the optical emission from artworks is the presence of multiple emitting compounds with spectra characterized by broad emission bands. The photoluminescence imaging methods here proposed allow to partially solve this issue, by separating emission from different materials on the basis of their different timescales and spectral emission properties, thus providing important information to support material identification. Furthermore, the high spectral accuracy achievable with a hyperspectral camera, such as the one proposed in this paper, allows the collection of highly resolved spectral datacubes, which can then be post-processed with computational and multivariate statistical analysis methods to better assess material identification and mapping.

## 1 Introduction

The identification of materials used in artworks is fundamental for establishing appropriate conservation procedures, for understanding the artistic techniques, for the correct dating of the artwork and for identifying past retouching and cleaning procedures. Recently, the demand for non-invasive and non-destructive techniques for the characterization of artistic

<sup>a</sup> e-mail: [daniela.comelli@polimi.it](mailto:daniela.comelli@polimi.it) (corresponding author)

materials has increasingly emerged, giving rise to the definition of multi-analytical protocols and to the development of innovative instrumentation [1–3].

In this context, hyperspectral imaging has become very popular as an effective method for the non-invasive investigation, documentation and diagnostics of cultural heritage [4, 5]. Hyperspectral imaging is often applied to the study of polychrome surfaces of small or medium size objects in museum collections [6]. More recently the method has been also effectively implemented in outdoor applications on large mural surfaces [7]. In the heritage science field, hyperspectral imaging is typically employed to detect and study light diffusely reflected by an artistic surface [6] with the aim of revealing preparatory sketches and hidden details [8, 9], of retrieving accurate color information and of achieving pigment identification and mapping. The experimental technique is often complemented by chemometric analysis methods [10–13]. More recently, hyperspectral imaging has been also applied to the analysis of photographic materials and their digitization and digital restoration [5]. Less commonly, hyperspectral imaging is applied to photoluminescence (PL) measurements to identify and map luminescent materials through their characteristic emissions, supporting the information obtained with other elemental and molecular spectroscopic analysis [10, 11, 14].

In recent years it has been demonstrated that the study of the photoluminescence emission from artworks and, more specifically, from paintings provides valuable information to detect and identify luminescent materials [15], to discriminate between pigments with similar composition but different production methods [16–18], to investigate the degradation processes occurring in oil paints [19–21], to highlight material heterogeneities at the microscale [16, 18, 22], to unravel features not visible with the naked eye [23] and to monitor the effectiveness of cleaning procedures [24]. Moreover, the high sensitivity of the luminescence techniques allows one to identify traces of luminescent materials not visible and/or not detectable by other non-invasive analytical methods [11, 25]. These studies clearly demonstrate the advantages of applying photoluminescence spectral techniques to the non-invasive and non-destructive study of cultural heritage objects.

In addition to the reconstruction of the spectral shape of the emission, the study of the temporal decay of luminescence adds important information, allowing one to distinguish different emitting materials or a material in different micro-environments on the basis of the emission lifetime [26]. However, due to the high sensitivity of the lifetime to the fluorophore micro-environment, this parameter can hardly be used for material identification. Instead, it can be particularly effective to combine temporal and spectral information of the luminescent emission under analysis: in this context, we recently demonstrated how time-gated multispectral photoluminescence imaging allows one to map luminescent materials emitting at different timescales in modern paintings and paint cross-sections [27–29].

In this work we further exploit this methodology by moving from a multispectral to a hyperspectral approach. For the purpose, we propose the use of a wide-field, compact and ultra-stable hyperspectral camera, based on the Fourier-transform approach, to accurately reconstruct and map emission spectra of luminescent pigments and paints occurring at different emission timescales. The hyperspectral imaging device, based on the Translating Wedge-based Identical pulse eNcoding System (TWINS) [30, 31], has been employed in the recent past to characterize steady-state photoluminescent emissions [32, 33]. Here, the TWINS interferometer is coupled first to a steady-state camera, and paint materials with different emission lifetimes are probed by varying the excitation fluence [34]. Then, the interferometer is coupled to a time-gated camera to map the spatial distribution of luminescent materials occurring at different timescales in both micro- and remote imaging modalities.

## 2 Experimental

### 2.1 Methods

#### 2.1.1 The TWINS interferometer

The TWINS system, fully described in a previously published patent [31] and papers [30, 32, 33], is a common-path birefringent interferometer that combines compactness (30 mm c.a. lateral dimension), intrinsic interferometric delay precision (1/360 of the optical cycle), long-term stability and insensitivity to vibrations. When it is placed in the optical path of an imaging system, the interferometer allows one to obtain high-quality interferograms for each point of the field of view. By means of the Fourier transform, the interferograms are then converted to high-quality spectra, which can arise from reflection, transmission or PL emission [32, 33]. The spectral resolution of the device is set by the maximum scan delay introduced by the interferometer and can be as good as 4 nm at 600 nm wavelength [32, 33].

#### 2.1.2 Steady-state hyperspectral micro-imaging coupled to double fluence excitation

Photoluminescence micro-imaging was performed by coupling the TWINS interferometer to a cooled monochrome camera (Retiga R6, Qimaging, spectral range 300–1000 nm). Two different lasers, with similar emission wavelengths but very different fluence values, have been employed in order to populate energetic levels with different population densities, and hence promoting de-excitation from different radiative and non-radiative decay decay paths [34]:

- i. A Q-switched Nd:YAG laser (CryLas FTSS 355–50, Crylas GmbH), emitting 1 ns pulses at 355 nm at a repetition rate of 100 Hz, with an average power density of 4 mW/mm<sup>2</sup> and a fluence per pulse (*i.e.*, in one nanosecond) of 4 mJ/cm<sup>2</sup>. Hereafter this laser excitation is designated as high-fluence (HF) excitation;
- ii. A compact CW laser (DL-375–015, CrystaLaser) with emission at 375 nm and a power density of 4 mW/mm<sup>2</sup> equivalent to a fluence in one nanosecond of 0.4 nJ/cm<sup>2</sup>. Hereafter this laser excitation is designated as low fluence (LF) excitation;

The two lasers can be conveyed alternately in a silica multi-mode optical fiber (600 μm core) by means of two interchangeable mirrors (Fig. 1a). The optical fiber is then coupled to a homemade microscope unit, working in epifluorescence configuration and equipped with a 50 × objective (PL FLUOTAR L 50 ×/0.55, Leica) and a dichroic mirror (Semrock, Brightline FF389-Di01). The micro-imaging system has a field of view of 250 μm in diameter and allows the analysis of micro-samples with a spatial sampling pitch of 0.2 μm. The acquisition protocol consists of recording two hyperspectral imaging datacubes of the same sample area alternatively excited with the LF and HF lasers.

#### 2.1.3 Time-gated hyperspectral camera

The TWINS interferometer is coupled to a time-gated intensified camera (C9546-03, Hamamatsu Photonics, and Retiga R6, Qimaging), with sensitivity in the 400–850 nm spectral range. Illumination is provided by the Q-switched Nd:YAG nanosecond pulsed laser, and synchronization between illumination and detection is provided by a precision delay generator (DG535, Stanford Research System) and a custom-built trigger unit.

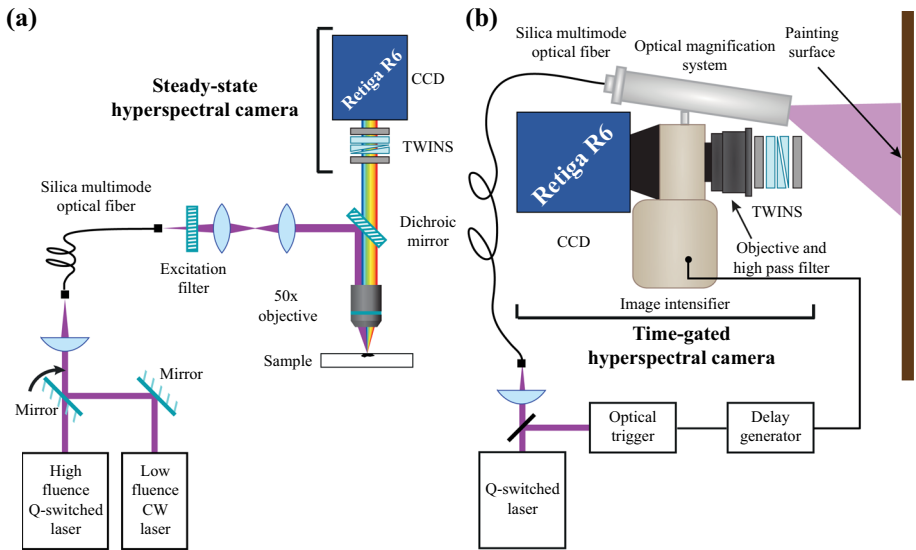


**Fig. 1** Scheme of the experimental setups. **a** Microscopy setup coupled with the two laser sources and the steady-state hyperspectral camera. **b** Time-gated hyperspectral setup employed for the remote imaging of paintings

The time-gated camera can be used for both micro-imaging of micro-samples and for the remote imaging of larger surfaces. In the first case, the hyperspectral camera is coupled to the microscope unit described in Sect. 2.1.2. In the second case, the time-gated camera is equipped with a 40 mm photographic objective (Schneider-Kreuznach), while the head of the excitation optical fiber is magnified and projected onto the surface under analysis through a magnifying optical system, to uniformly illuminate a circular area of about 10 cm in diameter. The spatial resolution of the system is essentially limited by the image intensifier (64 lp/mm on a photocathode of 17.5 mm in diameters), giving rise to a projected pixel of 0.1-mm-size over the illuminated area.

The acquisition protocol consists of recording two hyperspectral datacubes of the photoluminescence emission occurring at different delays after excitation: emissions at nanosecond timescale are probed by employing a gate window synchronous with the laser excitation, while longer emissions, at the microsecond timescale, are probed by using a gate window delayed by hundreds of nanoseconds with respect to the pulsed excitation.

#### 2.1.4 Data analysis protocol

Data analysis includes the reconstruction of the image of the RGB emission and the extraction of PL emission spectra in selected regions of interest (ROIs) of the analyzed samples. In the following, we report spectra averaged in selected ROIs, together with the corresponding standard deviation within the ROI (represented by shaded areas in the spectral plots). Spectra are corrected by the spectral efficiency of the detector, and the Jacobian factor required to convert the primary spectral quantity used by the instrument (wavenumber) into the more common wavelength.

Composite images are generated by merging spectral images detected in different bands in a false color representation. The identification of areas with similar spectral features is

obtained through the application of the spectral angle mapper (SAM) algorithm [35, 36], where PL spectra are treated as vectors, and the spectral similarity with a reference spectrum of interest is calculated as the angle between vectors. Pixels with similar emission spectra are grouped and displayed in a gray scale map, ranging from white (smallest angle value) to black (largest angle value).

## 2.2 Materials

Hyperspectral photoluminescence micro-imaging with double fluence excitation was tested (i) on a powder dispersion of pure zinc white pigment (ZnO, Kremer Pigmente GmbH) and (ii) on a paint stratigraphy, embedded in epoxy resin, taken from an unknown modern painting by Mikhail Larionov (sample L3, Archivio Gallone, Physics Department, Politecnico di Milano).

Time-gated hyperspectral imaging was performed in micro-imaging modality on a paint stratigraphy embedded in epoxy resin, taken from the painting *Allegoria in memoria di Francesca De Maestri Colleoni* by Arturo Albertazzi (Oil on canvas, 1909, Istituto dei Ciechi di Milano), and in remote imaging modality on two modern paintings: an untitled painting by the artist Borrelli (Oil on panel, 20 × 10 cm, 20th century, private collection) and a woman portrait by an unknown artist (Oil on canvas, 33 × 65 cm, 20th century, private collection).

## 3 Results

### 3.1 Hyperspectral photoluminescence micro-imaging with double fluence excitation

Two different excitation fluence values, provided by the LF and HF lasers, are exploited to highlight the presence of different recombination pathways in pigments and paints in micro-imaging mode [34]. The approach has been first tested on zinc white pigment powder (Fig. 2). Reconstructed RGB images of the emission clearly show the different luminescent behavior of the pigment under the two excitation regimes. Under HF excitation, zinc white exhibits a homogeneous and bright blue emission, corresponding to the Near Band-Edge (NBE) emission of the ZnO semiconductor [16, 37]. Indeed, HF excitation leads to saturation of trap states, as a consequence of their limited number and of the low rate of these de-excitation paths (*i.e.*, long decay time). Hence, the emission from other recombination channels, as the near band-edge direct recombination, become more probable [34, 37, 38]. In contrast, by reducing the excitation fluence, keeping constant the average irradiance, emission from trap states is detected. In this latter case, the emission is highly heterogeneous within the sample, and it is possible to distinguish blue and green emitting spots corresponding to the presence of different crystal defects in the ZnO crystal structure [16, 38]. By selecting different ROIs, it is possible to identify two distinctive emission peaks at 425 and 520 nm, that well correspond to trap state emissions reported by other authors in zinc white pigments [16]. By exploiting the SAM algorithm, it is possible to visualize the distribution of these emitting centers throughout the analyzed sample (Fig. 2c).

The study of a paint cross-section is displayed in Fig. 3. The paint stratigraphy L3 is composed of a thin brownish layer (layer 1), a white layer where coarse blue grains are dispersed (layer 2), a yellow layer (layer 3) and a light blue layer (layer 4). Details of the composition obtained by SEM-EDX data can be consulted in Ghirardello et al. [34].

All layers show a detectable PL signal in both excitation regimes. The accurate reconstruction of their emission spectra, made possible by the high spectral resolution achievable

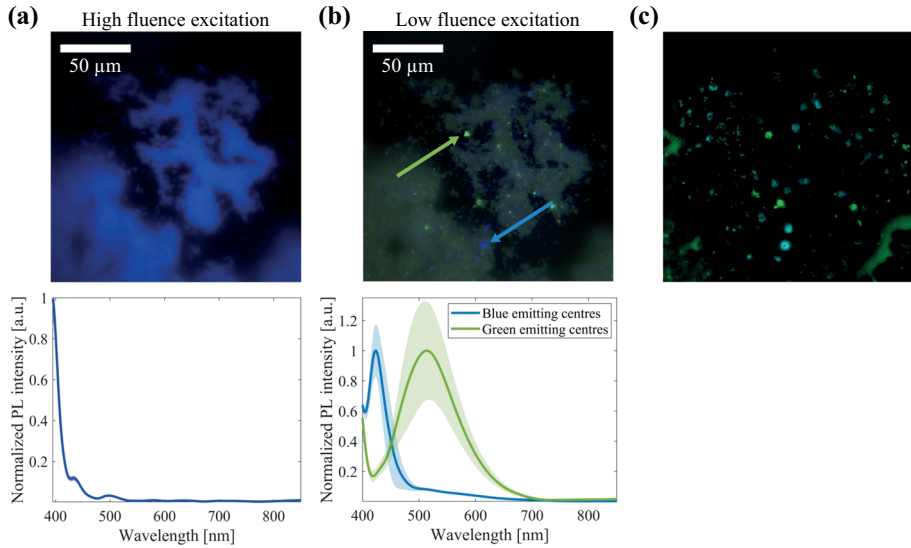


**Fig. 2** Zinc white pigment powder dispersion. **a** Reconstructed RGB image of the emission excited by the HF excitation (top panel) and mean emission spectrum recorded in the whole sample (bottom panel). **b** Reconstructed RGB image of the emission excited by the LF excitation (top panel) and selected spectra of green- and blue-emitting centers (bottom panel) recorded in the ROIs indicated by colored arrows and corresponding to the two different emitting centers. **c** False color image obtained by combining SAM maps, highlighting the presence of blue and green emitting centers. Angle values range between 0–35 degrees (blue-emitting centers) and 0–30 degrees (green emitting centers)

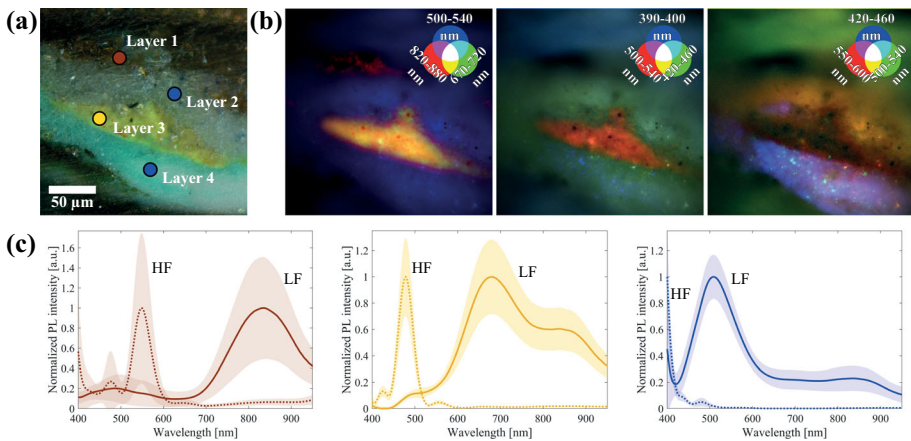


**Fig. 3** (a) Visible image of the stratigraphic cross-section L3 taken from a painting by Mikhail Larionov with indication of the 4 identified layers. **b** Different false color images of the emission obtained by combining images in different spectral bands extracted from the datacube obtained with low fluence excitation. Left panel: blue = 500–540 nm, green = 670–720 nm, red = 820–880 nm; Central panel: blue = 390–400 nm, green = 420–460 nm, red = 550–600 nm; Right panel: blue = 420–460 nm, green = 500–540 nm, red = 550–600 nm. **c** Normalized PL spectra, excited by the HF and LF excitation, in selected ROIs of the paint cross-section, as highlighted by the corresponding filled colored circles in the visible image. Dotted lines represent spectra obtained at HF excitation, continuous lines spectra obtained at LF excitation

with the TWINS interferometer, allows us to identify the luminescent pigments embedded in each layer (Fig. 3c). As stated, HF excitation mainly promotes near band-edge emission. Indeed, when employing this excitation in all paint layers we detect a narrow emission, centered, respectively, at 550 nm for layer 1, 480 nm for layer 3 and below 390 nm for layers 2 and 4. In contrast, with low fluence excitation, we detect broader and red-shifted emissions, ascribable to recombination from different trap states. On the basis of the recorded spectral features, we infer that paint layer 1 is made of cadmium sulfide (CdS) [39, 40], layer 3 of zinc cadmium sulfide (ZnCdS) [39, 40], while layers 2 and 4 are both made of zinc white pigment (ZnO) [16, 37] with the addition of non-emitting blue pigments.

An important advantage provided by hyperspectral imaging is the ability to reconstruct the emission intensity image in any spectral band within the analyzed spectral range and then combine the obtained spectral images into a false color representation. This allows one to visualize tiny differences of the emissions and highlight spatial heterogeneities within the sample. An example of different false color images is provided in Fig. 3b. The first image (left panel) has been obtained by selecting three spectral images at wavelengths corresponding to the trap state emission peaks of the identified pigments (blue channel: 500–540 nm for ZnO, green channel: 670–720 nm for ZnCdS, red channel: 820–880 nm for CdS). This image provides a clear visualization of the spatial distribution of these pigments within the paint layers. Central panel was obtained by merging spectral images corresponding to the NBE emission peak of ZnO (blue channel, 390–400 nm), ZnCdS (green channel, 420–460 nm) and CdS (red channel, 500–540 nm). Right panel was obtained by merging spectral images corresponding to the NBE emission peak of ZnCdS (blue channel, 420–460 nm), the NBE emission peak of CdS (green channel, 500–540 nm) and the emission in the 550–600 nm spectral range (red channel). Central panel highlights the presence of different emitting centers in ZnO layers (blue and green spots [16, 38]), and right panel allows one to identify a slight difference in the emission of the two ZnO-based paint layers (layer 2 and layer 4, right panel). Indeed, while layer 2 appears to have a higher contribution to the emission in the 550–600 nm spectral range, layer 4 has an emission in 420–460 nm spectral range, richer of different emitting centers.

### 3.2 Time-gated photoluminescence hyperspectral imaging

#### 3.2.1 Micro-imaging

A micro cross-section taken from the painting *Allegoria in memoria di Francesca De Maestri Colleoni* by Arturo Albertazzi was analyzed employing the microscopy setup coupled with the time-gated hyperspectral camera. The sample (Fig. 4a) shows a complex stratigraphy made of a thick white layer with a red line and yellowish particles dispersed (layer 1), a dark green layer (layer 2), a layer with blue and green particles dispersed in a white matrix (layer 3), a thin blue layer with reddish grains (layer 4) and a white ground layer (layer 5). Under common UV light (Fig. 4b), a greenish emission is observed in layers 1 and 3, a bright red emission is present at the interface between layers 4 and 5, and a white emission is observed from the ground layer (layer 5). Although UV photography allows one to highlight some differences between the paint layer, it does not provide clear information on the possible composition of the material.

Time-gated analysis of the photoluminescence emission occurring at nanosecond timescale allows the identification of three distinctive emissions: a strong emission occurring below 390 nm in layers 1 and 3; a two-band emission occurring at the interface of layers 4 and 5, peaked at ~470 and 600 nm, respectively; a broad emission distributed in the whole visible



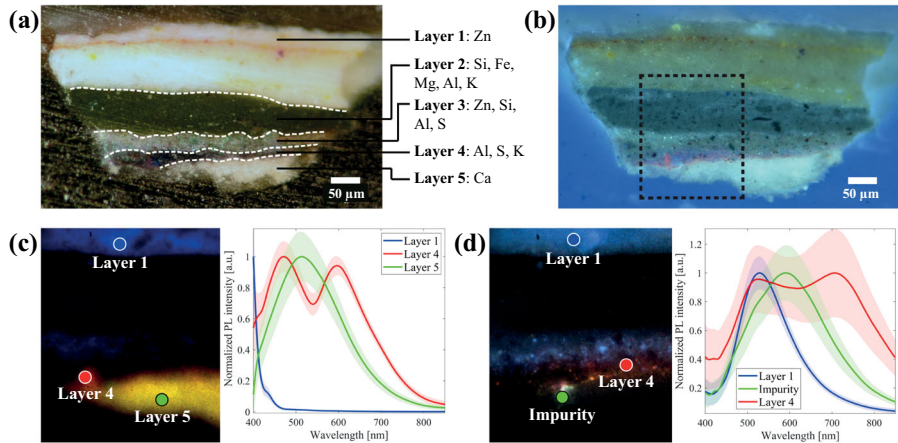


**Fig. 4** (a) Visible image of the micro-sample from *Allegoria in memoria di Francesca De Maestri Colleoni* by Arturo Albertazzi and main elements present in the layers as detected by SEM–EDS analysis. **b** UV image of the micro cross-section obtained with a benchtop microscope. The area highlighted by a black rectangle corresponds to results obtained by hyperspectral time-gated microscopy shown in panel (c) and (d). **c** False color image of the emission occurring at nanosecond timescale obtained by combining the emission in the band 390–400 nm (blue), 530–570 nm (green) and 595–615 nm (red) and reconstructed emission spectra in selected ROIs, corresponding to the filled colored circles. **d** False color image of the emission occurring at microsecond timescale obtained by combining the emission in the band 535–555 nm (blue), 600–650 nm (green) and 700–740 nm (red) and reconstructed emission spectra in selected ROIs, corresponding to the filled colored circles

range in layer 5. Three different spectral images in three spectral bands (390–400 nm = blue, 530–570 nm = green and 595–615 nm = red) were extracted from the hyperspectral dataset at nanosecond timescale and merged in false color representation (Fig. 4c) to highlight the distribution of the characteristic emissions.

Analysis at the microsecond timescale (Fig. 4d) reveals the presence of a broad emission peaked at ~530 nm in layers 1 and 3 and of a faint red emission (710 nm peak position) present as heterogeneous grains dispersed in layer 4. A further emitting impurity is detected at layers 4 and 5 interface, while no microsecond emission is detected in layer 5.

The emission detected in layers 1 and 3, present as a narrow peak at the nanosecond timescale and a broad emission at the microsecond timescale, corresponds to the typical emission of zinc white pigment [16, 37], as confirmed by SEM–EDS elemental map of the paint cross-section (see Supporting Information).

The red nanosecond emission peaked at 600 nm, detected at the interface of layer 4 and 5, can be associated to the presence of an organic colorant as red lake-based pigment, due to its fast emission decay and the good correspondence of this emission with the spatial distribution of alum [41] (see SEM–EDS elemental map in Supporting Information). The peak at ~470 nm can be instead ascribed to the binder. It is here noted that this nanosecond emission spatially differs from the microsecond emission peaked at 710 nm, that is present as heterogeneous coarse grains in layer 4. This suggests the presence of another emitting species. Elemental analysis has evidenced the presence of Al, S and K, suggesting the presence of a sulfur-containing sodium-silicate pigment as blue ultramarine pigment (confirmed also by Raman spectroscopy, see Supporting Information). Ultramarine pigment can be composed of different minerals (as *e.g.*, lazurite, calcite, pyrite, diopside, wollastonite and sodalite [42])



that could present different emissions due to impurities (see *e.g.*, sodalite and lazurite in Gaft et al. [43]). However, a further investigation is required to attribute the origin of such emission to a specific compound. Finally, the nanosecond emission of the ground layer, whose main element is calcium (see Supporting Information), could be related to the oleic binder due to its fast decay time.

### 3.2.2 Remote imaging of paintings

Time-gated hyperspectral PL imaging was applied to the analysis of two modern paintings. The first painting represents a fluvial landscape painted in light tones with colorful and golden details (Fig. 5a). Under UV light, the painting shows an intense bluish emission due to the varnish layer applied on painting surface (Fig. 5b). Time-gated hyperspectral imaging measurements at the nanosecond timescale (Fig. 5c) reveal a uniform emission of the painting, in which it is possible to recognize the emission of the varnish and the binder, broadly spread between 400 and 550 nm [26, 44], and the emission of zinc white pigment, due to the characteristic NBE emission occurring at 380 nm [37, 38] (Fig. 5f). Analysis of the emission at the microsecond timescale, when the fluorescence of the varnish, the oleic binder and the NBE emission of ZnO are completely decayed [26], allows the detection of an emission peaked at 530 nm, associated with trap state emissions of zinc white pigments [37, 38]. The distribution of zinc white trap states, achieved through SAM method (Fig. 5e), confirms that the pigment is spatially distributed in the whole painting.

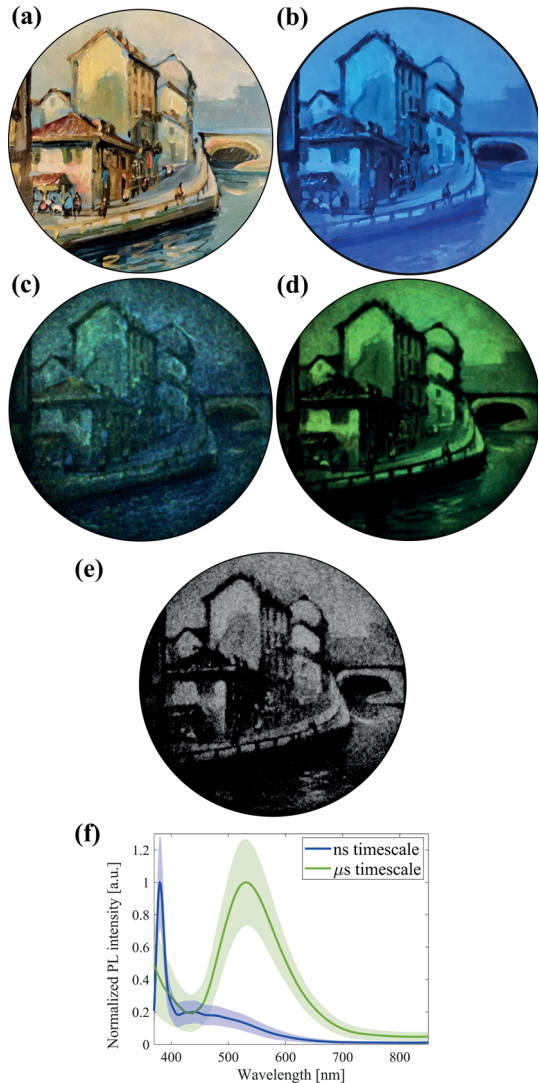
The second painting examined is a woman portrait. The analysis of the painting was performed to address the inquiry by conservators regarding the composition of the painting material, aimed at identifying the white pigment used for the skin. Indeed, elemental analysis made through the portable XRF mapping system (ELIO, XGLab srl—Bruker Nano Analytics) [45], infers the presence of titanium, zinc and barium, which are ascribed to different types of white pigments (see Supporting Information). Photoluminescence measurements, sensitive only to the most superficial paint layer, have been carried out in order to identify the pigment chosen by the artist to paint the skin tone. Results on an area corresponding to the face (Fig. 6) are here reported.

Nanosecond emission shows a broad emission distributed in the visible range, ascribed to the binder applied on the painting. Instead, an emission peaked in the near-infrared region (835 nm) occurs at the microsecond timescale. Such an infrared emission is peculiar of the rutile polymorph of titanium white pigment [17, 46]. Moreover, a good agreement between the emission in the 800–850 nm spectral band and the elemental distribution of titanium white is observed (Fig. 6c and d). Therefore, we can suppose that the figure was painted with titanium white paints, while the presence of zinc and barium, detected by XRF mapping, suggests the use of lithopone for the ground preparation of the canvas.

## 4 Discussion and conclusion

In general, PL imaging is considered a qualitative inspection technique for cultural heritage applications. However, recent studies employing PL spectral imaging at high spectral or spatial resolution have demonstrated that this optical method can provide information not achievable with other analytical techniques. For example, Dooley et al. [11], have employed PL spectral imaging to identify and map low concentrations of eosin lake in faded area of *The Olive Orchard* by Vincent Van Gogh, demonstrating that highly-sensitive fluorescence imaging spectroscopy, combined with multivariate analysis methods, can optimally complement

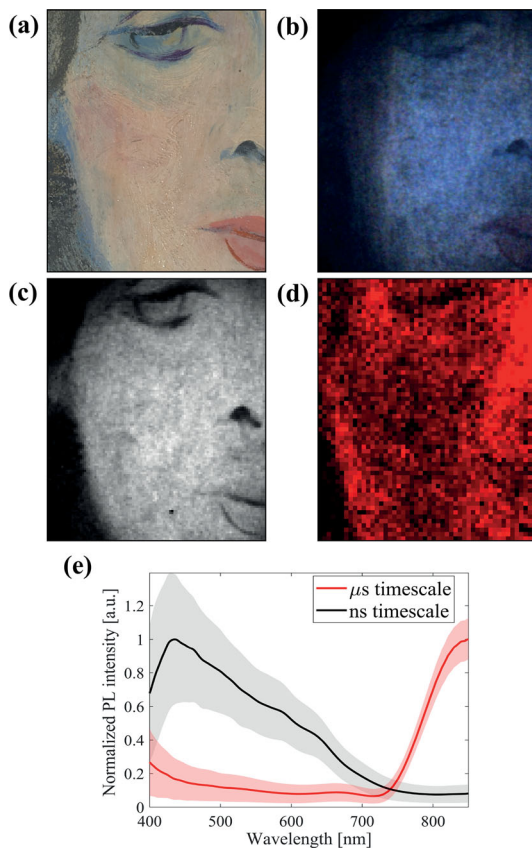
**Fig. 5** **a** Visible and **b** UV images of a detail of the painting by Borrelli. The area analyzed is a circular spot of 10 cm in diameter. **c** Reconstructed RGB emission at nanosecond and **d** microsecond timescale. **e** Similarity map, achieved with SAM method by considering as the reference spectrum the trap state emission of zinc white (green spectrum in panel (f)). Angle values range between 0 (white) and 20 (black) degrees. **f** Mean time-gated PL spectra reconstructed in the two temporal regimes of an area of the sky



other imaging spectroscopies. Other striking examples were provided by Thoury et al., who demonstrated how multispectral PL micro-imaging with sub-micrometric spatial resolution allows the identification of crystal defect fluctuations at the crystallite level, unraveling the coexistence of two hitherto indistinguishable non-stoichiometric cuprous oxide phases [22] in an archeological manufacture and the distribution of zinc soaps [19] in paints.

In this context, the two novel PL hyperspectral imaging techniques presented in this paper add a further step to the information achievable from PL studies. Indeed, the main difficulty when analyzing the PL emission from complex artworks is the presence of multiple emitting compounds, with broad emission bands and poorly characteristic emissions. The PL imaging methods here proposed allow us to partially overcome this issue, by separating emitting materials on the basis of their different timescales and spectral emission properties.

**Fig. 6** **a** Visible image of a detail of the woman portrait. **b** Reconstructed RGB emission at nanosecond timescale. **c** Spectral image at microsecond timescale in 800–850 nm spectral range. **d** Spatial distribution of titanium, based on the XRF counts at the Ti  $K\alpha$  emission line. **e** Average spectra extracted from an area corresponding to the cheek at the two different timescales



The excitation at two different fluence regimes is particularly interesting and little exploited in the field. The advantage of this approach is the possibility to use a digital steady-state camera, simpler and much cheaper than a time-gated detector. Further, steady-state cameras typically cover a broader spectral range and display a higher spectral resolution than the ones of a time-gated image intensifier. These advantages are clearly demonstrated by the high-quality of the images displayed in Figs. 2 and 3.

Nonetheless, the excitation at different fluence regimes cannot perfectly separate different recombination paths that instead can be well separated by using a time-gated camera. For example, the PL spectrum of zinc white excited by LF excitation displays both emissions from near band-edge and trap state recombination (Figs. 2 and 3), while when the same material is probed with the time-gated approach, the two paths are perfectly separated (Figs. 4 and 5). Moreover, the double fluence approach requires reaching a sufficiently high-fluence excitation in the analyzed area. This can be achieved only when the excitation spot is focused on an area of hundreds of micrometers in diameter, and hence, it can be employed only for micro-imaging of samples. Instead, the time-gated approach can be implemented also for the remote study of larger surfaces.

In conclusion, we have demonstrated the effectiveness and benefits of the TWINS hyper-spectral imaging system to probe luminescent emissions occurring in pigments and paints by coupling it with different excitation and detection schemes. We recall that this work is based

on the findings achieved in previous research, where we demonstrated the effectiveness of combining spectral and time-resolved information [27–29, 34] in PL imaging studies. Here, we have moved from a rough multispectral system to a hyperspectral one, and the benefits provided by the use of an hyperspectral approach are here reported:

- (i) The hyperspectral system allows us to measure PL spectra with a higher spectral resolution with respect to the previous multispectral one (based on 10 filters with FWHM of 40 and 50 nm step, covering the range between 400–850 nm [27, 28]), enhancing the method ability to identify luminescent materials.
- (ii) The high spectral resolution of the TWINS camera allows us to collect highly resolved spectral datacubes, which can then be post-processed with many computational methods with respect to the multispectral ones, commonly used for PL measurements [12, 14, 22, 27, 28, 47, 48]. For example, we have demonstrated how it is possible to reconstruct the image of the optical emission in any spectral band of interest (of any spectral width) and then combine them to highlight tiny differences within samples, as shown in Fig. 3b. Further, we have demonstrated how it is possible to exploit multivariate statistical analysis as the SAM supervised method, to map the spatial distribution of luminescent compounds. In future, further statistical analysis methods could be tested.
- (iii) The flexibility and compactness of the hyperspectral device allow us to easily couple it with both a standard CCD camera and a time-gated camera to perform steady-state and time-gated imaging. Moreover, the system has been both easily coupled to an optical microscope and employed for the remote imaging of artwork surfaces, making it a versatile device.

**Supplementary Information** The online version contains supplementary material available at <https://doi.org/10.1140/epjp/s13360-021-02028-0>.

**Acknowledgements** Authors wish to thank Dr. Carlotta Beccaria for providing the micro-sample from *Allegoria in memoria di Francesca De Maestri Colleoni* by Arturo Albertazzi (Istituto dei Ciechi di Milano), Ms. Beatrice Busetto for allowing the study of Borrelli painting, Mr. Marcel Mantovan, Mr. Manuel Mantovan and Mr. Marc Gelhaar for allowing the study of the second painting (portrait of a woman). Authors wish also to thank Dr. Sara Mosca for performing Raman measurements and Dr. Alessia Artesani for performing SEM-EDS measurements on the sample from *Allegoria in memoria di Francesca De Maestri Colleoni* by Arturo Albertazzi.

**Funding** Open access funding provided by Politecnico di Milano within the CRUI-CARE Agreement.

**Data availability** The datasets generated during and/or analyzed during the current study are available from the corresponding author on reasonable request.

**Open Access** This article is licensed under a Creative Commons Attribution 4.0 International License, which permits use, sharing, adaptation, distribution and reproduction in any medium or format, as long as you give appropriate credit to the original author(s) and the source, provide a link to the Creative Commons licence, and indicate if changes were made. The images or other third party material in this article are included in the article's Creative Commons licence, unless indicated otherwise in a credit line to the material. If material is not included in the article's Creative Commons licence and your intended use is not permitted by statutory regulation or exceeds the permitted use, you will need to obtain permission directly from the copyright holder. To view a copy of this licence, visit <http://creativecommons.org/licenses/by/4.0/>.

## References

1. B. Brunetti, C. Miliani, F. Rosi et al., Non-invasive investigations of paintings by portable instrumentation: The MOLAB experience. *Top Curr. Chem.* **374**, 1–35 (2016). <https://doi.org/10.1007/s41061-015-0008-9>
2. G.J. Tserovelakis, P. Pouli, G. Zacharakis, Listening to laser light interactions with objects of art: a novel photoacoustic approach for diagnosis and monitoring of laser cleaning interventions. *Herit. Sci.* **8**, 1–13 (2020). <https://doi.org/10.1186/s40494-020-00440-w>
3. M. Mari, G. Filippidis, Non-linear microscopy: A well-established technique for biological applications towards serving as a diagnostic tool for in situ cultural heritage studies. *Sustain* (2020). <https://doi.org/10.3390/su12041409>
4. H. Liang, Advances in multispectral and hyperspectral imaging for archaeology and art conservation. *Appl. Phys. A Mater. Sci. Process.* **106**, 309–323 (2012). <https://doi.org/10.1007/s00339-011-6689-1>
5. M. Picollo, C. Cucci, A. Casini, L. Stefani, Hyper-spectral imaging technique in the cultural heritage field: New possible scenarios. *Sens. (Switzerland)* (2020). <https://doi.org/10.3390/s20102843>
6. C. Cucci, J.K. Delaney, M. Picollo, Reflectance hyperspectral imaging for investigation of works of art: old master paintings and illuminated manuscripts. *Acc. Chem. Res.* **49**, 2070–2079 (2016). <https://doi.org/10.1021/acs.accounts.6b00048>
7. C. Cucci, M. Picollo, L. Chiarantini et al., Remote-sensing hyperspectral imaging for applications in archaeological areas: Non-invasive investigations on wall paintings and on mural inscriptions in the Pompeii site. *Microchem. J.* **158**, 105082 (2020). <https://doi.org/10.1016/j.microc.2020.105082>
8. P. Ricciardi, J.K. Delaney, L. Glinsman et al., Use of visible and infrared reflectance and luminescence imaging spectroscopy to study illuminated manuscripts: pigment identification and visualization of under-drawings. *O3A Opt. Arts, Archit. Archaeol. II* **7391**, 739106 (2009). <https://doi.org/10.1117/12.827415>
9. G. van der Snickt, K.A. Dooley, J. Sanyova et al., Dual mode standoff imaging spectroscopy documents the painting process of the Lamb of God in the Ghent Altarpiece by J. And H. Van Eyck. *Sci. Adv.* **6**, 1–11 (2020). <https://doi.org/10.1126/sciadv.abb3379>
10. J.K. Delaney, K.A. Dooley, R. Radpour, I. Kakoulli, Macroscale multimodal imaging reveals ancient painting production technology and the vogue in Greco-Roman Egypt. *Sci. Rep.* **7**, 1–12 (2017). <https://doi.org/10.1038/s41598-017-15743-5>
11. K.A. Dooley, A. Chieli, A. Romani et al., Molecular fluorescence imaging spectroscopy for mapping low concentrations of Red Lake pigments: Van Gogh's painting The Olive Orchard. *Angew Chemie-Int. Ed.* **59**, 6046–6053 (2020). <https://doi.org/10.1002/anie.201915490>
12. J.K. Delaney, J.G. Zeibel, M. Thoury et al., Visible and infrared imaging spectroscopy of picasso's harlequin musician: Mapping and identification of artist materials in situ. *Appl. Spectrosc.* **64**, 584–594 (2010). <https://doi.org/10.1366/000370210791414443>
13. T. Kleynhans, D.W. Messinger, J.K. Delaney, Towards automatic classification of diffuse reflectance image cubes from paintings collected with hyperspectral cameras. *Microchem. J.* **157**, 104934 (2020). <https://doi.org/10.1016/j.microc.2020.104934>
14. M. Thoury, J.K. Delaney, E.R. De La Rie et al., Near-infrared luminescence of cadmium pigments: In situ identification and mapping in paintings. *Appl. Spectrosc.* **65**, 939–951 (2011). <https://doi.org/10.1366/11-06230>
15. A. Romani, C. Clementi, C. Miliani, G. Favaro, Fluorescence spectroscopy: A powerful technique for the noninvasive characterization of artwork. *Acc. Chem. Res.* **43**, 837–846 (2010). <https://doi.org/10.1021/ar900291y>
16. L. Bertrand, M. Réfrégiers, B. Berrie et al., A multiscale photoluminescence approach to discriminate among semiconducting historical zinc white pigments. *Anal.* **138**, 4463 (2013). <https://doi.org/10.1039/c3an36874b>
17. B. van Driel, A. Artesani, K.J. van den Berg et al., New insights into the complex photoluminescence behaviour of titanium white pigments. *Dye Pigment* **155**, 14–22 (2018). <https://doi.org/10.1016/j.dyepig.2018.03.012>
18. M. Ghirardello, S. Mosca, J. Marti-Rujas et al., Time-resolved photoluminescence microscopy combined with X-ray analyses and raman spectroscopy sheds light on the imperfect synthesis of historical cadmium pigments. *Anal. Chem.* **90**, 10771–10779 (2018). <https://doi.org/10.1021/acs.analchem.8b01666>
19. S. Hageraats, K. Keune, M. Réfrégiers et al., Synchrotron deep-UV photoluminescence imaging for the submicrometer analysis of chemically altered zinc white oil paints. *Anal. Chem.* **91**, 14887–14895 (2019). <https://doi.org/10.1021/acs.analchem.9b02443>

20. D. Comelli, D. MacLennan, M. Ghirardello et al., Degradation of cadmium yellow paint: new evidence from photoluminescence studies of Trap States in Picasso's *Femme (époque des "demoiselles d'Avignon")*. *Anal. Chem.* **91**, 3421–3428 (2019). <https://doi.org/10.1021/acs.analchem.8b04914>
21. M. Thoury, L.A. Van, K. Keune et al., Photoluminescence micro-imaging sheds new light on the development of metal soaps in oil paintings, in *Metal Soaps in Art*, ed. by F. Casadio, K. Keune, P. Noble et al. (Springer International Publishing, Berlin, 2019), pp. 211–225. <https://doi.org/10.1007/978-3-319-90617-1>
22. M. Thoury, B. Mille, T. Séverin-Fabiani et al., High spatial dynamics-photoluminescence imaging reveals the metallurgy of the earliest lost-wax cast object. *Nat. Commun.* **7**, 1–8 (2016). <https://doi.org/10.1038/ncomms13356>
23. D. Comelli, A. Nevin, G. Valentini et al., Insights into Masolino's wall paintings in Castiglione Olona: Advanced reflectance and fluorescence imaging analysis. *J. Cult. Herit.* **12**, 11–18 (2011). <https://doi.org/10.1016/j.culher.2010.06.003>
24. P. Moretti, M. Iwanicka, K. Melessanaki et al., Laser cleaning of paintings: in situ optimization of operative parameters through non-invasive assessment by optical coherence tomography (OCT), reflection FT-IR spectroscopy and laser induced fluorescence spectroscopy (LIF). *Herit. Sci.* **7**, 1–12 (2019). <https://doi.org/10.1186/s40494-019-0284-8>
25. G. Verri, The spatially resolved characterisation of Egyptian blue, Han blue and Han purple by photo-induced luminescence digital imaging. *Anal. Bioanal. Chem.* **394**, 1011–1021 (2009). <https://doi.org/10.1007/s00216-009-2693-0>
26. A. Nevin, A. Cesaratto, S. Bellei et al., Time-resolved photoluminescence spectroscopy and imaging: new approaches to the analysis of cultural heritage and its degradation. *Sensors* **14**, 6338–6355 (2014). <https://doi.org/10.3390/s140406338>
27. M. Ghirardello, G. Valentini, L. Toniolo et al., Photoluminescence imaging of modern paintings: there is plenty of information at the microsecond timescale. *Microchem. J.* **154**, 104618 (2020). <https://doi.org/10.1016/j.microc.2020.104618>
28. D. Comelli, A. Artesani, A. Nevin et al., Time-resolved photoluminescence microscopy for the analysis of semiconductor-based paint layers. *Mater. (Basel)* **10**, 1–16 (2017). <https://doi.org/10.3390/ma10111335>
29. A. Artesani, M. Ghirardello, S. Mosca et al., Combined photoluminescence and Raman microscopy for the identification of modern pigments: explanatory examples on cross-sections from Russian avant-garde paintings. *Herit. Sci.* **7**, 1–13 (2019). <https://doi.org/10.1186/s40494-019-0258-x>
30. Brida D, Manzoni C, Cerullo G (2013) Phase-locked pulse pair for two-dimensional spectroscopy by a birefringent delay line. In: 2013 Conference Lasers Electro-Optics, CLEO 2013 37:3027–3029. [https://doi.org/10.1364/cleo\\_si.2013.cf2g.3](https://doi.org/10.1364/cleo_si.2013.cf2g.3)
31. Manzoni CA, Brida D, Cerullo GNF (2015) United States Patent US 9,182,284 B2
32. A. Perri, B.E. Nogueira de Faria, D.C.T. Ferreira et al., Hyperspectral imaging with a TWINS birefringent interferometer. *Opt. Express* **27**, 15956 (2019). <https://doi.org/10.1364/oe.27.015956>
33. A. Candeo, B.E. Nogueira De Faria, M. Erreni et al., A hyperspectral microscope based on an ultrastable common-path interferometer. *APL Photonics* (2019). <https://doi.org/10.1063/1.5129860>
34. M. Ghirardello, N.M. Kelly, G. Valentini et al., Photoluminescence excited at variable fluences: A novel approach for studying the emission from crystalline pigments in paints. *Anal. Methods* **12**, 4007–4014 (2020). <https://doi.org/10.1039/d0ay01160f>
35. F.A. Kruse, A.B. Lefkoff, J.W. Boardman et al., The spectral image processing system (SIPS)-interactive visualization and analysis of imaging spectrometer data. *Remote Sens. Environ.* **44**, 145–163 (1993). [https://doi.org/10.1016/0034-4257\(93\)90013-N](https://doi.org/10.1016/0034-4257(93)90013-N)
36. Harris Geospatial Solutions, Spectral Angle Mapper. Available online: <https://www.harrisgeospatial.com/docs/SpectralAngleMapper.html>. Accessed 12 Oct 2021
37. A. Artesani, S. Bellei, V. Capogrosso et al., Photoluminescence properties of zinc white: an insight into its emission mechanisms through the study of historical artist materials. *Appl. Phys. A Mater. Sci. Process.* (2016). <https://doi.org/10.1007/s00339-016-0578-6>
38. A. Artesani, M.V. Dozzi, L. Toniolo et al., Experimental study on the link between optical emission, crystal defects and photocatalytic activity of artist pigments based on zinc oxide. *Miner.* **10**, 1–15 (2020). <https://doi.org/10.3390/min10121129>
39. A. Cesaratto, C. D'Andrea, A. Nevin et al., Analysis of cadmium-based pigments with time-resolved photoluminescence. *Anal. Methods* **6**, 130–138 (2014). <https://doi.org/10.1039/C3AY41585F>
40. F. Rosi, C. Grazia, F. Gabrieli et al., UV-Vis-NIR and micro Raman spectroscopies for the non destructive identification of Cd<sub>1-x</sub>Zn<sub>x</sub>S solid solutions in cadmium yellow pigments. *Microchem. J.* **124**, 856–867 (2016). <https://doi.org/10.1016/j.microc.2015.07.025>



41. C. Clementi, B. Doherty, P.L. Gentili et al., Vibrational and electronic properties of painting lakes. *Appl. Phys. A Mater. Sci. Process* **92**, 25–33 (2008). <https://doi.org/10.1007/s00339-008-4474-6>
42. M. González-Cabrera, P. Arjonilla, A. Domínguez-Vidal, M.J. Ayora-Cañada, Natural or synthetic? Simultaneous Raman/luminescence hyperspectral microimaging for the fast distinction of ultramarine pigments. *Dye Pigment* (2020). <https://doi.org/10.1016/j.dyepig.2020.108349>
43. M. Gaft, R. Reisfeld, G. Panczer, *Modern Luminescence Spectroscopy of Minerals and Materials* (Springer International Publishing, Berlin, 2015). <https://doi.org/10.1007/978-3-319-24765-6>
44. E.R. de la Rie, E.R. de la Rie, Fluorescence of paint and varnish layers (Part III). *Stud. Conserv.* **27**, 102 (1982). <https://doi.org/10.2307/1506145>
45. <https://www.bruker.com/en/products-and-solutions/elemental-analyzers/micro-xrf-spectrometers/elio.html>
46. A. Artesani, S. Mosca, M.V. Dozzi et al., Determination of crystal phases in mixed TiO<sub>2</sub> paint films by non-invasive optical spectroscopies. *Microchem. J.* **155**, 104739 (2020). <https://doi.org/10.1016/j.microc.2020.104739>
47. C.S. Chane, M. Thoury, A. Tournie, J.P. Echard, Implementation of a neural network for multispectral luminescence imaging of lake pigment paints. *Appl. Spectrosc.* **69**, 430–441 (2015). <https://doi.org/10.1366/14-07554>
48. M. Thoury, J.P. Echard, M. Réfrégiers et al., Synchrotron UV-visible multispectral luminescence microimaging of historical samples. *Anal. Chem.* **83**, 1737–1745 (2011). <https://doi.org/10.1021/ac102986h>